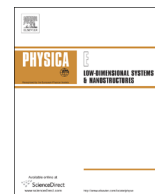




ELSEVIER

Contents lists available at ScienceDirect

Physica E

journal homepage: [www.elsevier.com/locate/phys](http://www.elsevier.com/locate/phys)

# Spin- and valley-polarized transport through ferromagnetic and antiferromagnetic barriers on monolayer MoS<sub>2</sub>

P.M. Krstajić<sup>a,\*</sup>, P. Vasilopoulos<sup>b</sup>, M. Tahir<sup>b</sup><sup>a</sup> Institute of Microelectronic Technologies and Single Crystals (IHTM), University of Belgrade, Njegoševa 12, 11000 Belgrade, Serbia<sup>b</sup> Department of Physics, Concordia University, 7141 Sherbrooke Ouest, Montréal, Québec, Canada H4B 1R6

## HIGHLIGHTS

- We study electron transport through single/double barriers on monolayer MoS<sub>2</sub>.
- The conductance  $g_c$  and the polarization oscillate with barrier width  $d$ .
- The conductance versus ferromagnetic field  $M$  decreases in a fluctuating manner.
- The spin polarization  $P_s$  oscillates as a function of  $M$  before it becomes 100%.
- As for AFM barriers the conductance exhibits an oscillating behavior for  $d > 20$  nm.

## ARTICLE INFO

### Article history:

Received 11 August 2015

Received in revised form

25 September 2015

Accepted 1 October 2015

Available online 5 October 2015

### Keywords:

Quantum transport

Low dimensional physics

Nanostructures

## ABSTRACT

We study ballistic electron transport through single or double barriers on monolayer MoS<sub>2</sub>, of width  $d$ , in the presence of a ferromagnetic field  $M$  or an antiferromagnetic field  $F$ . The total conductance  $g_c$ , its spin-up and spin-down components, and the polarization oscillate with  $d$  or the distance  $b$  between two barriers. The corresponding oscillation periods are different. The conductance  $g_c$  versus  $M$  decreases in a fluctuating manner with a steep decline at certain value of  $M$ . As a function of  $M$  the spin polarization  $P_s$  oscillates before it becomes 100% while the valley polarization  $P_v$  oscillates and steadily increases.

© 2015 Elsevier B.V. All rights reserved.

## 1. Introduction

Since its discovery graphene has attracted a remarkable attention due to its exotic properties and potential applications in various fields [1]. Still there remain fundamental problems due to its zero band gap and weak spin-orbit interaction (SOI). These problems could be overcome by, e.g., using silicene, the silicon analog of graphene, a similar material called germanene, or MoS<sub>2</sub> and other dichalcogenide materials, all of them promising candidates for the next generation nanoelectronic devices [2–5]. A review of silicene's properties is given in Ref. [6]. Here we focus on MoS<sub>2</sub>, a semiconducting analogue of graphene, which has a honeycomb structure similar to graphene's [7]. In addition though, it has a huge intrinsic direct band gap, 1.66 eV wide, and a very large SOI  $2\lambda = 150$  meV [7,8]. This strong SOI can lead to spin- and valley-polarized transport and the energy dispersion may be

manipulated as recent works indicate [9–11]. Such a transport has been studied in silicene, in which the SOI strength is 3.9 meV, in the presence of exchange fields and led to novel spin and valley polarizations [12,13]. Given the huge gap and very strong SOI in MoS<sub>2</sub>, we expect to find significant differences in similar studies. Here we study spin- and valley-polarized transport through ferromagnetic (FM) and antiferromagnetic (AFM) barriers in MoS<sub>2</sub>.

The paper is organized as follows. In Section 2 we present the basic expressions for ballistic transport through FM barriers as well as the results for the conductance and polarizations. In Section 3 we do the same for AFM barriers, and in Section 4 we present our conclusions.

## 2. Ferromagnetic (FM) barriers

We consider a monolayer of MoS<sub>2</sub> in the  $(x,y)$  plane. Particles in MoS<sub>2</sub> are described by the two-dimensional (2D) Dirac-type Hamiltonian [14–16]

\* Corresponding author.

E-mail addresses: [predrag222@gmail.com](mailto:predrag222@gmail.com) (P.M. Krstajić),  
[p.vasilopoulos@concordia.ca](mailto:p.vasilopoulos@concordia.ca) (P. Vasilopoulos),  
[m.tahir06@alumni.imperial.ac.uk](mailto:m.tahir06@alumni.imperial.ac.uk) (M. Tahir).

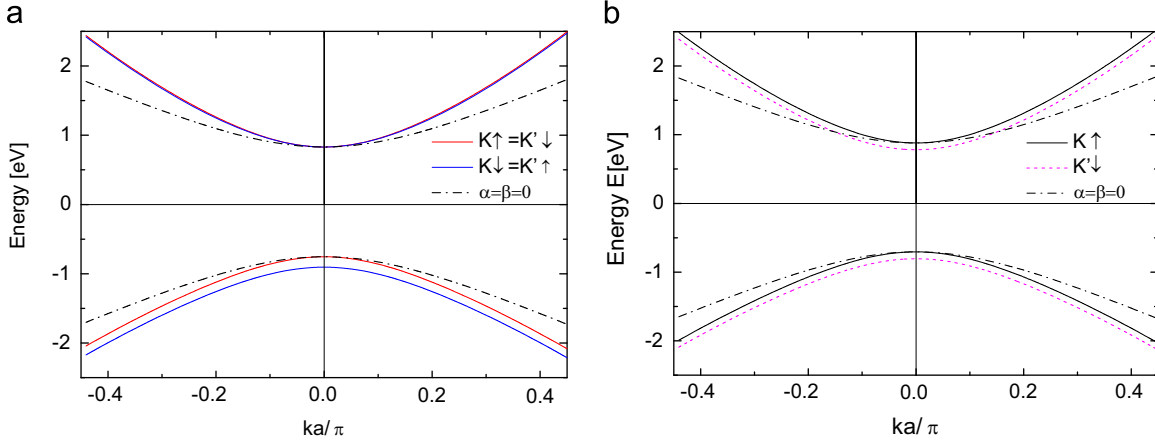


**Fig. 1.** Energy dispersion for  $M_z = 0$  in (a) and  $M_z = 50$  meV in (b). Further,  $\Delta' = 830$  meV,  $\lambda' = 37.5$  meV,  $\alpha = 0.43$  and  $\beta = 2.21$ . The dash-dotted black curve is the spectrum for  $\alpha = \beta = 0$ .

$$H_{S_z}^{\eta} = v(\eta\sigma_x p_x + \sigma_y p_y) + \Delta' \sigma_z + (I - \sigma_z)\eta s_z \lambda' + \frac{\hbar^2 k^2}{4m_0}(\alpha I + \beta \sigma_z) + s_z M_z. \quad (1)$$

Here  $\eta = \pm 1$  for valleys  $K$  and  $K'$ ,  $\Delta' = \Delta/2$ ,  $\Delta$  is the mass term that breaks the inversion symmetry,  $\lambda' = \lambda/2$ ,  $\lambda$  is the SOI strength,  $\sigma_i$ ,  $i = x, y, z$ , are the Pauli matrices for the valence and conduction bands, and  $I$  is the identity matrix. The  $\alpha$  term takes into account the difference between electron and hole masses, and the  $\beta$  term leads to new topological phenomena. Further,  $s_z = 1$  ( $-1$ ) for spins up (down), and  $v$  denotes the Fermi velocity of the electrons.  $M_z$  is the exchange field. The eigenvalues pertaining to Eq. (1) are

$$E_{S_z, t}^{\eta} = \eta s_z \lambda' + s_z M_z + \frac{\alpha \hbar^2 k^2}{4m_0} + t [c_k^2 + \Delta_{\xi}^2]^{1/2} \quad (2)$$

where  $c_k = \hbar v k$ ,  $\Delta_{\xi} = \Delta' - \lambda' \xi + \frac{\beta \hbar^2 k^2}{4m_0}$ ,  $\xi = \eta s_z$ . The energy dispersion is shown in Fig. 1(a) for  $M_z = 0$ , and in Fig. 1(b) for  $M_z = 50$  meV. The dash-dotted black curve is for  $\alpha = \beta = 0$ . The gap is  $2\Delta'$ , with  $\Delta' = 830$  meV, SOI constant  $\lambda' = 37.5$  meV, and  $\alpha = 0.43$ ,  $\beta = 2.21$  (Ref. [16]).

The corresponding eigenfunctions are written as

$$\Psi_{S_z, t}^{\eta} = e^{i\mathbf{k}\cdot\mathbf{r}} \begin{pmatrix} \frac{\eta C_k e^{-i\eta\phi}}{D_{\xi k}} \\ -\frac{\Delta_{\xi} - t\delta_{\xi k}}{D_{\xi k}} \end{pmatrix}, \quad (3)$$

where

$$D_{\xi k} = [c_k^2 + (\Delta_{\xi} - t\delta_{\xi k})^2]^{1/2}, \quad \delta_{\xi k}^2 = c_k^2 + \Delta_{\xi}^2. \quad (4)$$

For electrons it is  $t=+1$  and for holes  $t = -1$ .

First we consider a FM barrier of width  $d$  (region II) between two normal regions (I and III) of MoS<sub>2</sub>. The eigenfunctions in regions I, II, and III are

$$\Psi_I(\mathbf{r}) = \mathbf{e}^{i\mathbf{k}\cdot\mathbf{r}} \begin{pmatrix} A_1 e^{-i\eta\theta} \\ B_1 \end{pmatrix} + \mathbf{r}_{\eta s_z} \mathbf{e}^{i(-k_x x + k_y y)} \begin{pmatrix} A_1 e^{-i\eta(\pi-\theta)} \\ B_1 \end{pmatrix}, \quad (5)$$

$$\Psi_{II}(\mathbf{r}) = \mathbf{p} e^{i(q_x x + k_y y)} \begin{pmatrix} A_2 e^{-i\eta\phi} \\ B_2 \end{pmatrix} + \mathbf{q} e^{i(-q_x x + k_y y)} \begin{pmatrix} A_2 e^{-i\eta(\pi-\phi)} \\ B_2 \end{pmatrix}, \quad (6)$$

$$\Psi_{III}(\mathbf{r}) = \mathbf{t}_{\eta s_z} \mathbf{e}^{i\mathbf{k}\cdot\mathbf{r}} \begin{pmatrix} A_1 e^{-i\eta\theta} \\ B_1 \end{pmatrix}. \quad (7)$$

Here  $r_{\eta s_z}$  and  $t_{\eta s_z}$  are the reflection and transmission coefficients.

Further  $A_i$ , and  $B_i$  are eigenvector components pertinent to Eq. (3), that is  $A_1 = \eta \hbar v (k_x^2 + k_y^2)^{1/2}$ ,  $A_2 = \eta \hbar v (q_x^2 + k_y^2)^{1/2}$ , and  $B_1 = -(\Delta_{\xi} - t\delta_{\xi k}(k_x, k_y))/D_{\xi k}(k_x, k_y)$ , while  $B_2 = -(\Delta_{\xi} - t\delta_{\xi k}(q_x, k_y))/D_{\xi k}(q_x, k_y)$ . Note that the angles  $\theta$  and  $\phi$  are the angles the momentum makes with the  $x$ -axis,  $\theta = \arctan(k_y/k_x)$ , and  $\phi = \arctan(k_y/q_x)$ . Due to the translational invariance the transverse momentum is conserved, i.e.,  $k'_y = k_y$ . The transmission amplitude is found from the continuity of the wave functions  $\Psi_I(x=0, y) = \Psi_{II}(x=0, y)$  and  $\Psi_{II}(x=d, y) = \Psi_{III}(x=d, y)$ . The resulting transmission reads

$$T_{\eta s_z}(\theta) = 1/\left[1 + \sin^2(q_x d)(F^2(\gamma, \theta, \phi) - 1)\right], \quad (8)$$

with  $\gamma = k_F(\Delta_{\xi}' - t\delta_{\xi k}')/(k_F(\Delta_{\xi} - t\delta_{\xi k}))$ ,  $q_x = k_F \cos \phi$ , and  $F(\gamma, \theta, \phi) = (\gamma + \gamma^{-1} - 2 \sin \theta \sin \phi)/2 \cos \theta \cos \phi$ . The transmission becomes unity  $T_{\eta s_z} = 1$  for  $q_x d = n\pi$ ,  $n = 1, 2, \dots$ , regardless of the values of the angles  $\theta$  and  $\phi$  as in graphene. On the other hand, for normal incidence we have  $\theta = \phi = 0$ , the transmission acquires the form

$$T_{\eta s_z}(0) = 1/[1 + \sin^2(q_x d)(\gamma - \gamma^{-1})^2/4], \quad (9)$$

and is less than unity. Apart from notation Eq. (9) is the same as that of Ref. [13] and for  $\lambda' = M_z = 0$  we have  $\gamma = 1$  and  $T_{\eta s_z}(0) = 1$  as in graphene independent of the values of  $\sin^2(q_x d)$ .

With  $G_0 = e^2 k_F W / 2\pi \hbar$ , the conductance due to a particular spin and valley is given by

$$G_{\eta s_z} = G_0 \int_{-\pi/2}^{+\pi/2} T_{\eta s_z}(\theta) \cos \theta d\theta = G_0 g_{c\eta s_z}, \quad (10)$$

where  $W$  is the width along the  $y$  direction. In Fig. 2(a) we show the total conductance  $g_c$  (black curve) and its spin-up (red dotted curve) and spin-down (blue dotted curve) components as functions of the barrier width  $d$  of the FM junction. The Fermi energy was taken to be  $E_F = 0.9$  eV and the exchange energy  $M_z = 50$  meV. As expected the conductances oscillate with the barrier width  $d$  but the oscillations are denser for spin-down conductance. In Figs. 2(b) and (c) we plot the spin polarization  $P_s = (g_{\uparrow} - g_{\downarrow})/(g_{\uparrow} + g_{\downarrow})$  and valley polarization  $P_v = (g_K - g_{K'})/(g_K + g_{K'})$  versus the width  $d$ . All other parameters are the same as those for Fig. 2(a).  $P_s$  exhibits an oscillatory behavior while the height of the peaks tends to decrease with  $d$ . As shown,  $P_v$  is of the same order of magnitude as  $P_s$ , visibly non-monotonic, and rather irregular.

Further, in Fig. 3 we show the total conductance  $g_c$  versus the ratio  $M/\lambda'$  for fixed barrier width  $d=25$  nm. In general the conductance oscillates with  $M$ , while there is a sharp decline at around  $M = 1.75\lambda'$ . Similar oscillations, but narrowing with  $M$  appear in  $P_s$  before it becomes perfect for a wide range of  $M$  while

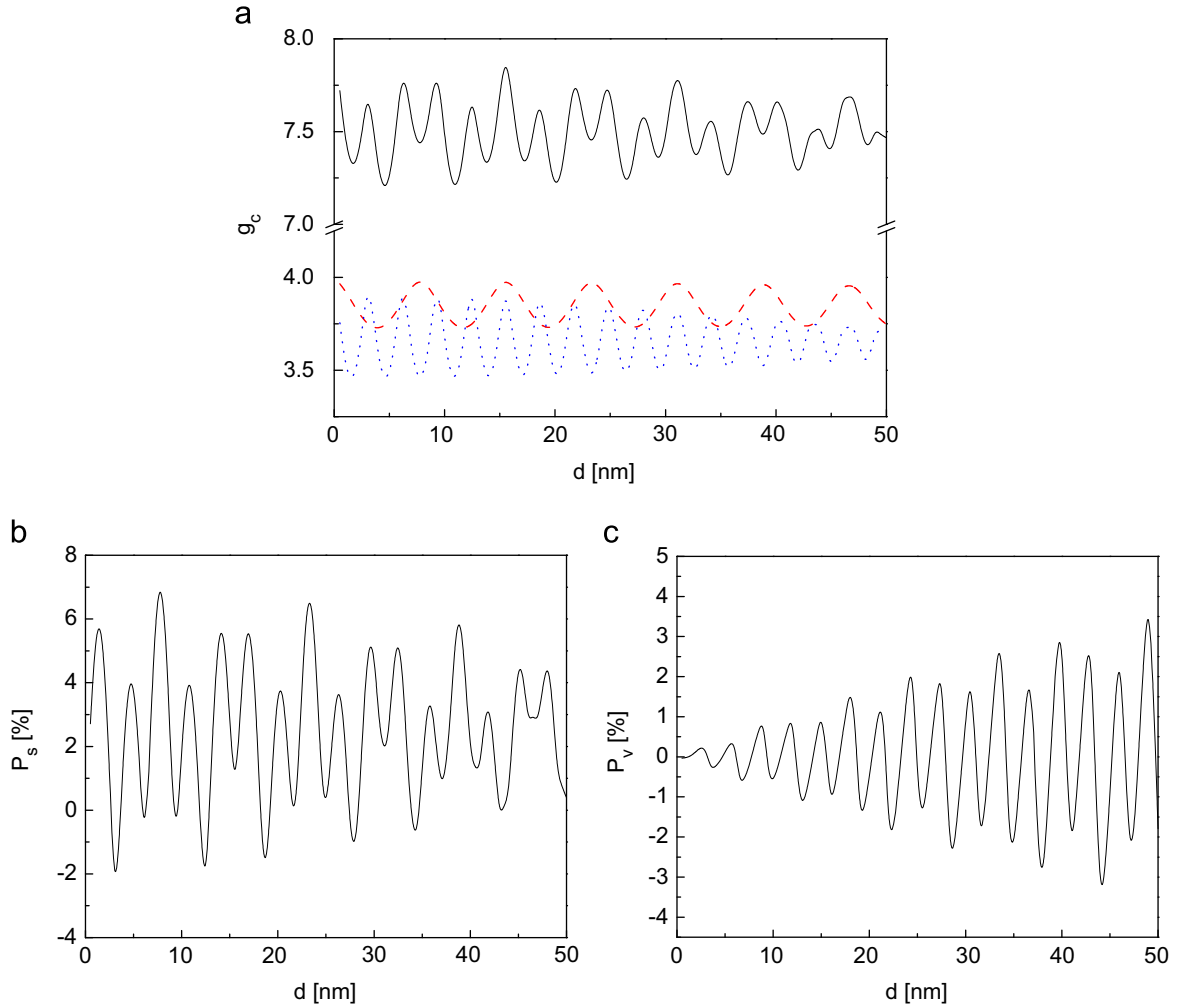


**Fig. 2.** (a) Total (black curve), spin-up (red dashed curve) and spin-down (blue dotted curve) conductances versus the width  $d$  of the FM layer. (b) Spin polarization  $P_s$  and (c) valley polarization  $P_v$ , versus the width  $d$  for  $E_F = 0.9$  eV and  $M_z = 50$  meV. (For interpretation of the references to color in this figure caption, the reader is referred to the web version of this paper.)

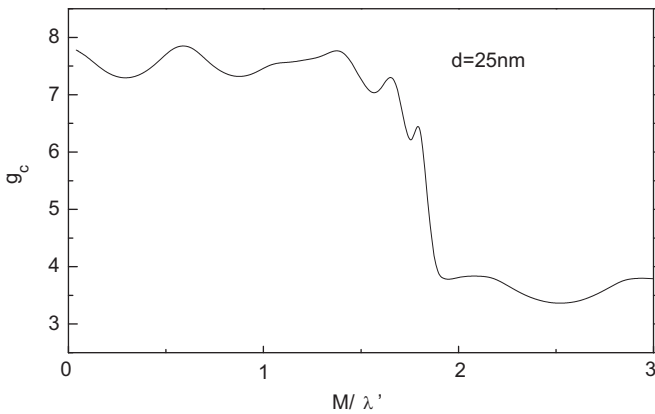


**Fig. 3.** Conductance  $g_c$  as a function of the exchange energy  $M$  for  $E_F = 0.9$  eV.

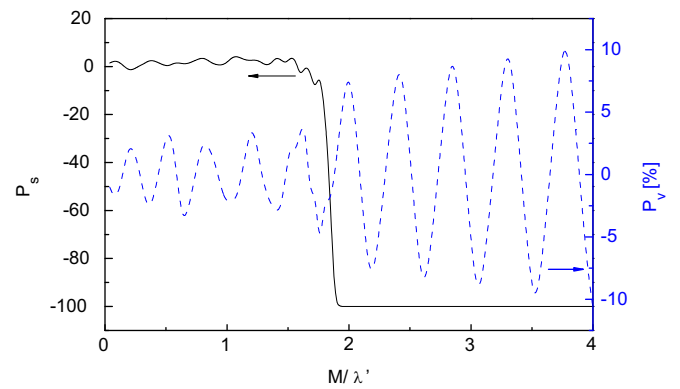


**Fig. 4.** Spin ( $P_s$ , solid curve) and valley ( $P_v$ , dashed curve) polarizations versus  $M/\lambda'$  for  $d=50$  nm. The left scale is for  $P_s$  and the right one for  $P_v$ .

$P_v$  oscillates with  $M$  and is smaller than  $P_s$ . We show that in Fig. 4 where we plot  $P_s$  (solid curve) and  $P_v$  (dashed curve) versus  $M/\lambda'$  with the left-axis scale for  $P_s$  and the right one for  $P_v$ .

To check the influence of the Fermi energy on the conductance, in Fig. 5 we plot  $g_c$  (black curve),  $g_\uparrow$  (red dashed curve), and  $g_\downarrow$  (blue dotted curve) as functions of  $E_F/\lambda'$ . All curves start around  $E_F = 23\lambda$ , since only then do we have a nonzero propagating wave vector  $k_x$ . It can be seen that  $g_c$  increases rapidly around  $E_F = 25\lambda$ .

For larger values of  $E_F$  the spin-up component tends to reach the spin-down one, as the field  $M$  becomes negligible compared to  $E_F$ .

Next, we consider two identical FM layers separated by an ordinary MoS<sub>2</sub> layer of width  $b$ . First, in Fig. 6 we present the polarization  $P_s$  versus the FM layers' width  $d$  for fixed  $b=50$  nm. Comparing the results with those for the single barrier in Fig. 2(b), one sees that the shape is similar, a more complex oscillating behavior stemming from different Fermi wave vectors for spin-up

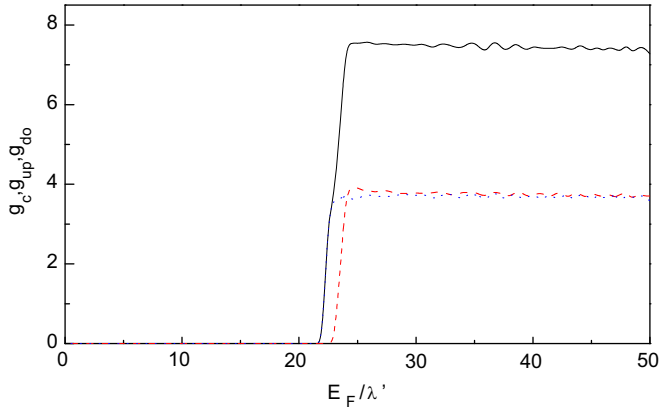


**Fig. 5.** Total conductance  $g_c$  (black curve),  $g_\uparrow$  (red dashed curve) and  $g_\downarrow$  (blue dotted curve) versus  $E_F/\lambda'$  ( $d=50$  nm). (For interpretation of the references to color in this figure caption, the reader is referred to the web version of this paper.)

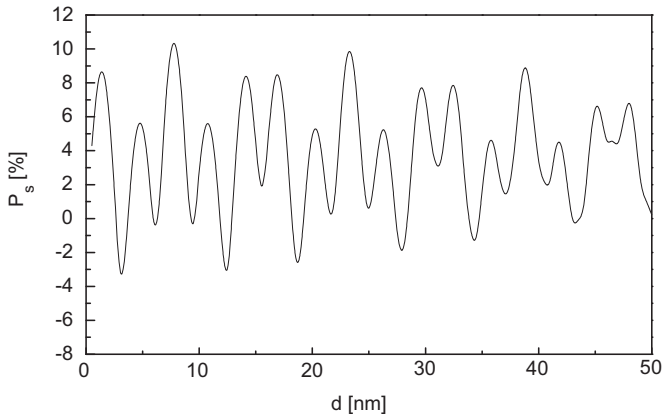


**Fig. 6.** Spin polarization  $P_s$  in a double FM barrier versus the width  $d$  for barrier separation  $b=50$  nm ( $E_F = 0.9$  eV).

and spin-down electrons. On the other hand, in Fig. 7(a) we plot the conductance  $g_c$  and in Fig. 7(b) the polarization  $P_s$  versus the separation  $b$  for fixed barrier width  $d=50$  nm. Both quantities oscillate with  $d$  but for  $d \geq 3$  nm  $P_s$  can change sign. Note that making the change  $M_z \rightarrow -M_z$  will change the role of spin-up and spin-down electrons, so that the total conductance will remain the same but  $P_s$  will change sign.

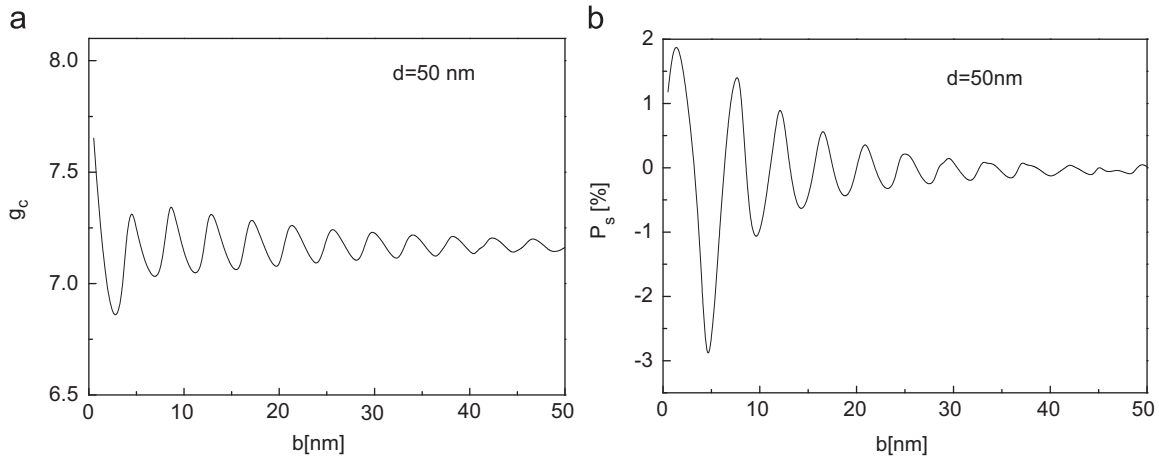


**Fig. 7.** (a) Conductance  $g_c$  through a double FM barrier versus their separation  $b$  for width  $d=50$  nm. (b) The corresponding spin polarization  $P_s$  ( $E_F = 0.9$  eV).

### 3. AFM barriers

We consider a monolayer of MoS<sub>2</sub> in  $(x, y)$  plane in the presence of an intrinsic SOI. Particles in MoS<sub>2</sub> obey the 2D, Dirac-type Hamiltonian

$$H_{s_z}^\eta = v(\eta\sigma_x p_x + \sigma_y p_y) + (\Delta' + F s_z)\sigma_z + (I - \sigma_z)\lambda'\eta s_z + \frac{\hbar^2 k^2}{4m_0}(\alpha I + \beta\sigma_z). \quad (11)$$

$F$  is the AFM field and all other symbols have the same meaning as in Eq. (1). The eigenvalues of Eq. (11) are

$$E_{t^{s,z}}^{\eta} = \eta s_z \lambda' + \frac{\alpha^2 \hbar^2 k^2}{4m_0} + t [c_k^2 + \Delta_{F\xi}^2]^{1/2}, \quad (12)$$

where  $\Delta_{F\xi} = \Delta' - \eta s_z \lambda' + s_z F + \beta \hbar^2 k^2 / (4m_0)$  and  $c_k = \hbar v k$ , as in the FM case. The corresponding eigenfunctions are

$$\psi_{s,t}^\eta = e^{i\mathbf{k}\cdot\mathbf{r}} \begin{pmatrix} \frac{\eta c_k e^{-i\eta\varphi}}{D_{F\xi k}} \\ -\frac{\Delta_\xi - t\delta_{\xi k}}{D_{F\xi k}} \end{pmatrix}, \quad (13)$$

where  $D_{F\xi k} = [c_k^2 + (\Delta_{F\xi} - t\delta_{\xi k})^2]^{1/2}$  and  $\delta_{\xi k}^2 = c_k^2 + \Delta_\xi^2$ .

In Fig. 8(a) we show the total conductance  $g_c$  (black curve), its spin-up (red dashed curve) and spin-down (blue dotted curve) components as functions of the width  $d$  for  $E_F = 0.9$  eV and  $F = 75$  meV. The total conductance exhibits an oscillating behavior for  $d > 20$  nm and the local maxima tend to be smaller with the increase of the width  $d$ . In Fig. 8(b) we present the calculated polarization  $P_s$  through the AFM layer versus the width  $d$ . As seen,  $P_s$  the polarization is very small for  $d < 5$  nm, while above 20 nm it saturates to nearly 100%.

As just seen, some results for a single AFM barrier are similar to those for a FM barrier. The same holds between the results of Figs. 3–7 and those corresponding to a double AFM barrier and will not be repeated. We hope that they will be tested by experiments.

### 4. Summary and concluding remarks

We reported new oscillations of the conductances and of the spin ( $P_s$ ) and valley ( $P_v$ ) polarizations through single and double FM or AFM barriers on monolayer MoS<sub>2</sub>, as functions of the barrier width or barrier separation.  $P_s$  shows a complex oscillating behavior vs barrier width  $d$  stemming from different Fermi wave

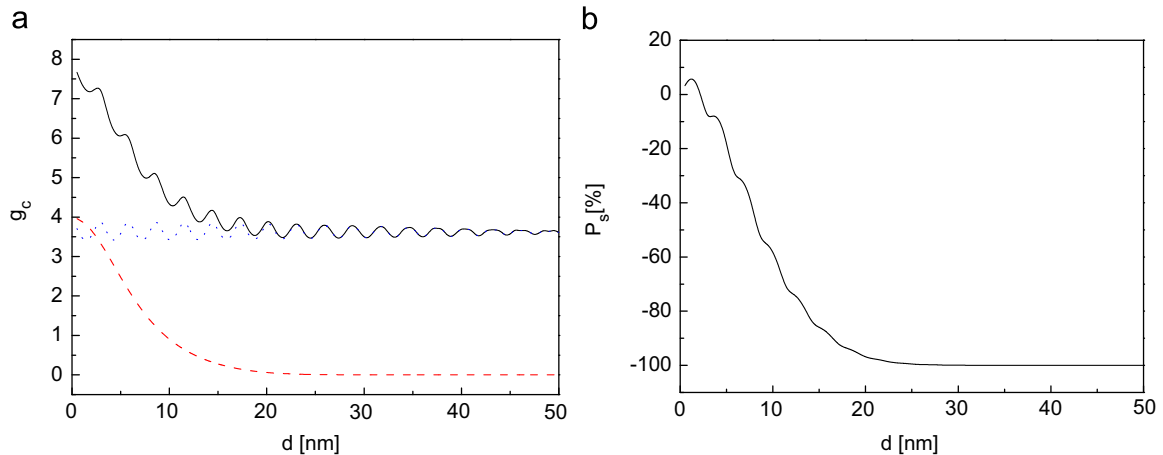


**Fig. 8.** (a) Total  $g_c$  (black curve), spin-up (red dashed curve), and spin-down (blue dotted curve) conductances through a AFM barrier versus its width  $d$ . (b) Polarization  $P_s$  versus  $d$  ( $E_F = 0.9$  eV and  $F = 75$  meV). (For interpretation of the references to color in this figure caption, the reader is referred to the web version of this paper.)

vectors for spin-up and spin-down electrons. On the other hand,  $P_v$  is of the same magnitude as  $P_s$  and increases with the width  $d$ . We also reported an oscillating behavior of the conductance versus the field  $M$  or  $F$  and an increase above a threshold value of the density or Fermi energy tied to its large mass term  $\Delta$ . A similar oscillating behavior is shown by  $P_s$  and a fluctuating one by  $P_v$ .

Two remarks are in order about the results. The first concerns the various oscillations of the conductances and of the polarizations, when the barrier width or barrier separation is varied. We emphasize that they are different from those of the transmission resulting from the maxima and minima of the term  $\sin^2(q_x d)$  in Eq. (8). Though not shown, this is evident from the integrated transmission in Eq. (10).

Another remark is about the influence of the  $\alpha$  and  $\beta$  terms in Eq. (1). The main results remain qualitatively the same, if we set  $\alpha = \beta = 0$ , but some quantitative changes occur and show the importance of these terms. Apart from the change in the spectrum shown in Fig. 1, the oscillations in  $P_v$  in Fig. 4 have an amplitude about a factor of two smaller than those for  $\alpha = \beta = 0$ . Similarly, the overall conductance versus barrier width increases, for  $\alpha \neq 0$  and  $\beta \neq 0$ , by nearly a factor of two, cf. Fig. 2, while versus  $M$ , cf. Fig. 3, the changes are more pronounced. We hope that the results will be tested by experiments.

## Acknowledgments

This work was supported by the Serbian Ministry of Education

and Science, within the Project no. TR 32008 (PK) and by the Canadian NSERC Grant no. OGP0121756 (PV, MT).

## References

- [1] C. Lee, Q. Li, W. Kalb, X.Z. Liu, H. Berger, R.W. Carpick, J. Hone, *Science* 328 (2010) 76.
- [2] A. Splendiani, L. Sun, Y. Zhang, T. Li, J. Kim, C.Y. Chim, G. Galli, F. Wang, *Nano Lett.* 10 (2010) 1271.
- [3] K.F. Mak, C. Lee, J. Hone, J. Shan, T.F. Heinz, *Phys. Rev. Lett.* 105 (2010) 136805.
- [4] B. Radisavljevic, A. Radenovic, J. Brivio, V. Giacometti, A. Kis, *Nat. Nanotechnol.* 6 (2011) 147.
- [5] T. Korn, S. Heydrich, M. Hirmer, J. Schmutzler, C. Schüller, *Appl. Phys. Lett.* 99 (2011) 102109; B. Radisavljevic, M.B. Whitwick, A. Kis, *Appl. Phys. Lett.* 101 (2012) 043103.
- [6] A. Kara, H. Enriquez, A.P. Seitsonen, L.C. Lew Yan Voon, S. Vizzini, B. Aufray, H. Oughaddoub, *Surf. Sci.* 67 (2012) 1.
- [7] D. Xiao, G.-B. Liu, W. Feng, X. Xu, W. Yao, *Phys. Rev. Lett.* 108 (2012) 196802.
- [8] Z.Y. Zhu, Y.C. Cheng, U. Schwingenschlögl, *Phys. Rev. B* 84 (2011) 153402.
- [9] T. Cao, G. Wang, W. Han, H. Ye, C. Zhu, J. Shi, Q. Niu, P. Tan, E. Wang, B. Liu, J. Feng, *Nat. Commun.* 3 (2012) 887.
- [10] K.F. Mak, K. He, J. Shan, T.F. Heinz, *Nat. Nanotechnol.* 7 (2012) 494; H. Zeng, J. Dai, W. Yao, D. Xiao, X. Cui, *Nat. Nanotechnol.* 7 (2012) 490.
- [11] G. Sallen, L. Bouet, X. Marie, G. Wang, C.R. Zhu, W.P. Han, Y. Lu, P.H. Tan, T. Amand, B.L. Liu, B. Urbaszek, *Phys. Rev. B* 86 (2012) 081301(R).
- [12] T. Yokoyama, *Phys. Rev. B* 87 (2013) 241409(R); T. Yokoyama, *New J. Phys.* 16 (2014) 085005.
- [13] V. Vargiamidis, P. Vasilopoulos, *Appl. Phys. Lett.* 105 (2014) 223105; V. Vargiamidis, P. Vasilopoulos, *J. Appl. Phys.* 117 (2015) 094305.
- [14] A. Kormányos, V. Zólyomi, N.D. Drummond, P. Rakyta, G. Burkard, V.I. Fal'ko, *Phys. Rev. B* 88 (2013) 045416.
- [15] H. Rostami, A.G. Moghaddam, R. Asgari, *Phys. Rev. B* 88 (2013) 085440.
- [16] L. Majidi, M. Zare, R. Asgari, *Solid State Commun.* 199 (2014) 52.